European Journal of Molecular & Clinical Medicine
ISSN 2515-8260 Volume 07, Issue 07, 2020

An Effective Segmentation Based on Optimized Kapur's Entropy with ANFIS Classification Model using MRI Images

Deeparani K[1], Sudhakar P[2]

[1]*Research Scholar, Department of Computer Science, Bharathiar University, Coimbatore-641 046, TN, India.*

[2]*Associate Professor, Department of Computer Science, Annamalai University, Chidambaram-TN, India.*

[1]*deeparanikannan@gmail.com*

[2]*kar.sudha@gmail.com*

*Abstract**: Image processing acts as a vital part of distinct healthcare applications to assist the computer based disease diagnosis models. The brain tumor is found to be a life-threatening kind of cancer and the earlier identification results in improved survival rate. Magnetic Resonance Image (MRI) is the commonly available imaging technique used for recording the glioma for the medical examination. Brain tumor segmentation and classification processes aim to separate the tumor from the normal brain tissues and identify the presence of brain tumor or node, which is helpful for further treatment. But it remains a crucial process owing to the irregular form and unclear boundaries of tumors. This paper presents a novel Optimized Kapur's Entropy with adaptive neuro fuzzy inference system (OKE-ANFIS) model for brain tumor segmentation and classification using MRI images. The presented model involves skull stripping based preprocessing, segmentation, and classification. The presented model employs OKE based segmentation technique where the optimal choice of threshold values is decided using moth flame optimization (MFO) algorithm. Besides, histogram of gradients (HOG) based feature extractor is employed. In addition, ANFIS based classifier is utilized to determine the class label of the applied MRI images. For experimental validation of the OKE-ANFIS model, a wide range of simulations was performed and the results are investigated under several aspects. The experimental outcome ensured the superiority of the OKE-ANFIS model.***

Keywords: Brain tumor, image segmentation, image classification, Kapur's entropy, Thresholding, ANFIS

1. INTRODUCTION:

A brain tumor (BT) defines a collection of abnormal cells which gets reproduced in the brain uncontrollably. The BT is normally categorized into two types namely benign and malignant. The former type is non-aggressive, developed gradually, and stays isolated from the nearby normal tissues [1]. At the same time, it is not distributed to other parts of the brain or other organs in the body and it is simpler to remove through the surgical process. On the other hand, the latter type does not easily differentiate from the nearby normal tissues. So, it is quite complicated to filter them with no harm to the nearby brain tissues. In addition, people infected by BT get increased day by day. Magnetic Resonance Imaging (MRI) is a non-invasive medical

imaging model widely employed to generate high resolution and high contrast among the soft tissues. It provides detailed data regarding the shapes, sizes, and localization of the BT to accurately diagnose it. So, several research studies on the diagnosis and classification of BT make use of MRI images [2, 3].

Several versions of MRI have been produced named as weighted images. Some of them are T1- weighted, T2-weighted, Proton-Density Weighted, and Fluid Attenuated Inversion Recovery (FLAIR). The first T1-weighted image gives an effective segmentation for brain tissue owing to the maximum contrast amongst the gray and white matters [4]. Next, the T1-weighted contrast-improved images and FLAIR are commonly utilized for BT structure diagnosis since it results in intensive tumor regions. The precise segmentation of BT using MRI images denotes an important and crucial process to diagnose and treat it. Image segmentation is a hot research area in the field of medical images that comprises extraction of images from the target regions. A different set of algorithms are available in the earlier works to detect BT namely thresholding [5, 6], region based, deformable, classification, and deep learning (DL) based models.

The deformable techniques remain effective to segment the BT using MRI images. It is identified using the curves (2D) or surfaces (3D) represented in the image which moves through the effect of two forces such as internal or local forces defined in the curve for making the deformation procedure smoother. At the same time, the external force is determined using the images for moving the curve in the direction of the object boundaries. At the deformable techniques, they are categorized into parametric deformable [7] and geometric deformable techniques. The first type of model requires a parametric representation at the time of deforming the curve. It has the tediousness in the modification in topology for splitting and merging the contours from the segmentation of many objects. The geometric deformable technique depends upon the geometric readings namely curve normal and curvature. The benefit of the model is the ability to adapt with the topological modifications at the time of curve propagation. The segmentation process comprises the extraction of tumor regions from the normal brain tissue and the occurrence of the BT is identifiable. But the precise and proficient segmentation of BT still remains a crucial process as they are in distinct shapes, sizes, and positions.

Earlier research works on the diagnosis of BT using MRI images depends upon several image processing techniques [18-24]. The advanced MRI examination processes comprise a neural network (NN) based model [8], watershed segmentation, clustering technique, fuzzy c-means, edge detection model, Adaptive Neuro Fuzzy Inference System (ANFIS) technique, Gaussian mixture model, cellular automata, multilevel thresholding, and heuristic algorithms. In addition, [9] highlighted the integration of different models for achieving effective segmentation performance. Apart from the NN models [10, 11], major of the above-mentioned segmentation techniques are modality based techniques and performs proficiently with the brain MRI registered with a specific modality. Therefore, a design of novel BT segmentation technique is suggested for the MRI data which is defined using a set of modalities namely FLAIR, spin lattice relaxation (T1), T1-contrast enhanced (T1C), and spin relaxation (T2).

This paper presents a novel Optimized Kapur's Entropy with adaptive neuro fuzzy inference system (OKE-ANFIS) model for brain tumor (BT) segmentation and classification using MRI images. The presented model involves skull stripping based preprocessing, segmentation, and classification. The presented model employs OKE based segmentation technique where the optimal choice of threshold values is decided using moth flame optimization (MFO) algorithm. Besides, histogram of gradients (HOG) based feature extractor is employed. In addition, ANFIS based classifier is utilized to determine the class label of the applied MRI images. To

ensure the goodness of the OKE-ANFIS model, a wide range of simulations were performed and the results are investigated under several aspects.

2. THE PROPOSED OKE-ANFIS MODEL

Fig. 1 showcases the working principle of the OKE-ANFIS model. The figure demonstrated that the OKE-ANFIS model initially performs the skull stripping process. Next, the preprocessed image undergoes OKE with MFO algorithm based image segmentation process to identify the affected portions in the MRI image. Finally, the HOG based feature extraction and ANFIS classifier get executed to allocate the proper class labels of the applied MRI test image.

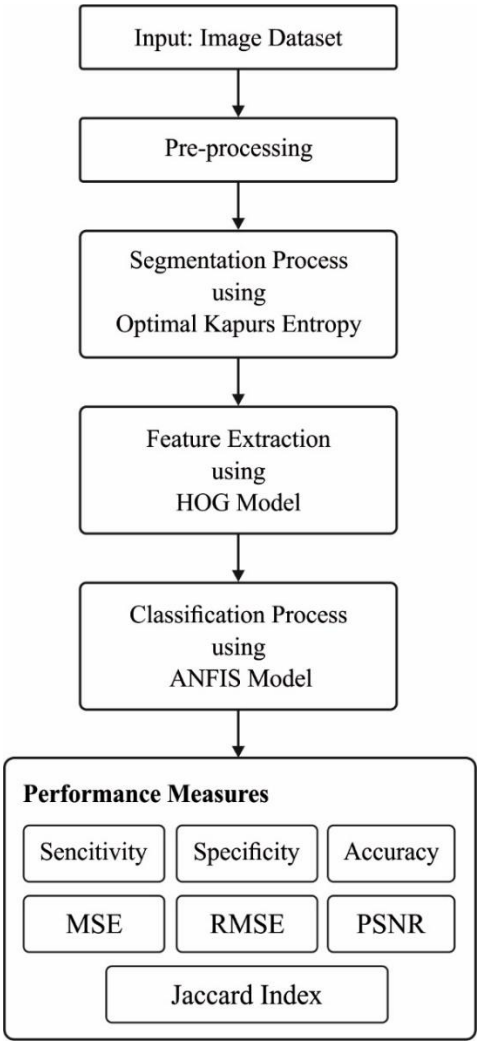

Fig. 1 Block diagram of OKE-ANFIS Model

A. Skull Stripping Process

It is the primary process mainly involved in the segmentation of the MRI images. It is essential to remove the skull from the backdrop region from the MRI to segment it. It is generally carried out using an imaging filter that separates the skull and the remaining portions of the image are masked with identical levels of intensities. On the applied MRI, generally, the

regions of skull or bones compass a higher threshold value (threshold>200) over the tumor and extra brain portions. Therefore, the image filtering technique is employed for the separation of the brain areas using a selected threshold value. Next to that, the skull gets stripped from the MRI using the solidity property.

B. Image Segmentation

For image segmentation, Kapur's entropy based multi-level segmentation process is employed. It is applied for finding the optimum threshold values to segment the images. It depends upon the entropy and probability distribution of the histogram. It is applied for the identification of the optimum (th) which maximizes the total entropy. In case of bi-level images, the objective function of Kapur's problem is represented by:

$$F_{kapur}(th) = H_1 + H_2 \tag{1}$$

where the entropies H_1 and H_2 are determined using Eq. (2):

$$H_1 = \sum_{i=1}^{th} \frac{Ph_i}{\omega_0} ln\left(\frac{Ph_i}{\omega_0}\right) \; and \; H_2 = \sum_{i=th+1}^{L} \frac{Ph_i}{\omega_1} ln\left(\frac{Ph_i}{\omega_1}\right) \tag{2}$$

where Ph_i is the probability distribution of the intensity levels attained, $\omega_0(th)$ and $\omega_1(th)$ are the probabilities distribution for the classes C_1 and C_2. $ln(.)$ is the natural logarithm. Comparable to the Otsu's technique, the entropy based model is altered for the multi-thresholding values and it is essential to partition the images into k class labels by the use of $k-1$ threshold values. The objective function can be changed using Eq. (3):

$$F_{kapur}(TH) = \sum_{i=1}^{k} H_i \tag{3}$$

where $TH = [th_1, th_2, \dots th_{k-1}]$ is a vector which comprises several multiple threshold values. All the entropies are determined individually with the corresponding (th) value, therefore, Eq. (3) is expanded for k entropies.

$$H_k^c = \sum_{i=th_{k+1}}^{L} \frac{Ph_i}{\omega_{k-1}} ln\left(\frac{Ph_i}{\omega_{k-1}}\right) \tag{4}$$

At this point, the probability occurrence $(\omega_0^c, \omega_1, \dots, \omega_{k-1})$ value of the k class labels are attained and the probability distribution Ph_i. For the optimal selection of threshold values, MFO algorithm is employed.

MFO is developed by S. Mirjalili [12]. A moth is an interesting creature which comprises the unique steering method during nighttime called transverse positioning technique. They fly during night time by saving a predefined angel based on the location of the moon. The identical principle gets employed by the moth for navigation purposes over the artificial light sources. They have managed to save a similar angle based on the human made light source. Therefore, they get stuck into a deadly spiral route over the artificial lights.

A mathematical representation of these characteristics is given below. Two main elements have existed in the MFO algorithm namely moth and flame. It is a population based metaheuristic algorithm. The element moth can be defined in the way of matrix, as given below:

$$M = \begin{bmatrix} m_{11} & m_{12} & \cdots & \cdots & m_{1d} \\ m_{21} & m_{22} & \cdots & \cdots & m_{2d} \\ \vdots & \vdots & \vdots & \vdots & \vdots \\ \vdots & \vdots & \vdots & \vdots & \vdots \\ m_{n1} & m_{n2} & \cdots & \cdots & m_{nd} \end{bmatrix} \tag{5}$$

where d represents the dimensions and n indicates the moth count. It is considered that the moth is assumed as the candidate solution and the location of the moth in the space is treated as the problem variable. For every moth, an array is available to store the respective values as given below.

$$OM = \begin{bmatrix} OM_1 \\ OM_2 \\ \vdots \\ \vdots \\ OM_n \end{bmatrix} \tag{6}$$

Another major element is the collection of flames that can be defined in the matrix format, as given below.

$$F = \begin{bmatrix} f_{11} & f_{12} & \cdots & \cdots & f_{1d} \\ f_{21} & f_{22} & \cdots & \cdots & f_{2d} \\ \vdots & \vdots & \vdots & \vdots & \vdots \\ \vdots & \vdots & \vdots & \vdots & \vdots \\ f_{n1} & f_{n2} & \cdots & \cdots & f_{nd} \end{bmatrix} \tag{7}$$

Likewise, an array is also existed to store the respective fitness value as given below:

$$OF = \begin{bmatrix} OF_1 \\ OF_2 \\ \vdots \\ \vdots \\ OF_n \end{bmatrix} \tag{8}$$

A major consideration is that the moths as well as flames are treated as solutions [13]. Although the major variation is process of creating and updating the candidate solution of moth and flame. On the applied MFO algorithm, the flame indicates the optimal position of the moth attained and the moth is considered as the actual searching agent which moves from one to other search spaces. As a result, the flames are the pins which are thrown by the moth at the time of exploring the searching area. The moths have tried to identify a flame and update the location for the identification of optimum solutions. It assists the moth to achieve effective solutions. As defined previously, the locations of the moths are updated based on the location of the flame, as given below.

$$M_p = S(M_p, F_q) \tag{9}$$

where M_p and F_q denotes the p-th moth and q-th flame correspondingly while S is the spiral function. The logarithmic spiral function indicates the major updating strategy of moth and is defined by

$$S(M_p, F_q) = D_p * e^{bt} * \cos(2\pi t) + F_q \tag{10}$$

where b specifies a constant for substantial modeling of the shapes of the logarithmic spiral, t is an arbitrary number that lies in the interval of [−1, 1] and D_p denotes the distance of the p_{th} moth for the q_{th} flame that is computed by

$$D_p = |F_q - M_p| \tag{11}$$

The above equation allows a moth to fly over the flame in a spiral way and not mainly in the gap amongst them. It assures the exploration and exploitation tasks of the search space. The exploration process takes place if the subsequent position exists exterior to the searching area amongst the moth and flame. At the same time, the exploitation takes place if the subsequent position is located in the space amongst the flame and moth. The moths are compelled for updating the location using any flame in Eq. (11). Then, the flames are arranged and categorized based on the fitness value in all iterations. Afterward, the moth updates the

locations depending upon the respective flames. It is essential to defined the flame count N at the start of the initial iteration. But at the completing levels of the rounds, the moth gets to update the position based on the optimal flame. So, the flame count gets decreased. For addressing this issue, an adaptive strategy is presented for decrementing the flame count and flame count gets reduced using Eq. (12):

$$flame\_no = round\left(N - l * \frac{N-1}{T}\right) \tag{12}$$

where l is the present round, N is the maximum flame count, and T denotes the maximum iteration count. The decrease in flame count balances the tradeoff among the exploitation and exploration of the searching area.

C. Feature Extraction

The segmented image is fed into the HOG technique to extract a useful set of feature vectors. A main characteristic of HOG is appropriate to get a local appearance of object and assume the invariance of object transformations and illumination conditions as edges and data regarding the gradients are validated by the use of many coordinate-HOG feature vectors. In addition, the gradient operator N is applied for determining the gradient value. A gradient point of image can be defined by G and image frame is represented by I. The common form of employing processing gradient point is defined below.

$$G_x = N * I(x,y) and\ G_x = N^T * I(x,y) \tag{13}$$

The image prediction window is categorized into spatial regions known as cells. Therefore, the magnitude gradients of pixels are performed with the direction of edges. At last, the magnitude of the gradient (x, y) can be defined as

$$G_x(x,y) = \sqrt{G_x(x,y)^2} + \sqrt{G_y(x,y)^2} \tag{14}$$

The edge orientation of point (x, y) can be equated in Eq. (15):

$$\theta(x,y) = \tan^{-1}\frac{G_y(x,y)}{G_x(x,y)} \tag{15}$$

Where Gx and Gy define the horizontal as well as vertical direction of the gradients.

D. ANFIS based Classification

At the final stage, the classification of BT using the segmented image takes place using ANFIS model. The filtered feature vectors from the HOG technique are applied for the classification of MRI images. They are collectively treated as the feature vectors with N feature count for the healthy and Glioma brain MRI images. They are given as input to the ANFIS model for differentiating the normal and abnormal MRI image. The classifier model is selected to obtain maximum detection rate. To achieve proficient classification performance, ANFIS model is employed that operates on low as well as high intensity Glioma brain MRI images. The ANFIS model involves individual input and output layers with 5 intermittent hidden layers. The neuron count in the input layer is found to be identical to the feature count in the filtered feature vector. The hidden layers comprise a set of ten neurons and are predefined for numerous rounds for obtaining maximum detection rate. The output layer has an individual neuron that generates the binary low and high depending upon the extracted feature vectors from the MRI images. The presented ANFIS model has the ability to determine the appropriate class label for the applied MRI.

3. PERFORMANCE VALIDATION

The performance of the OKE-ANFIS model is validated using a set of benchmark MRI images [14]. The results are examined interms of diverse aspects such as segmentation and classification outcomes.

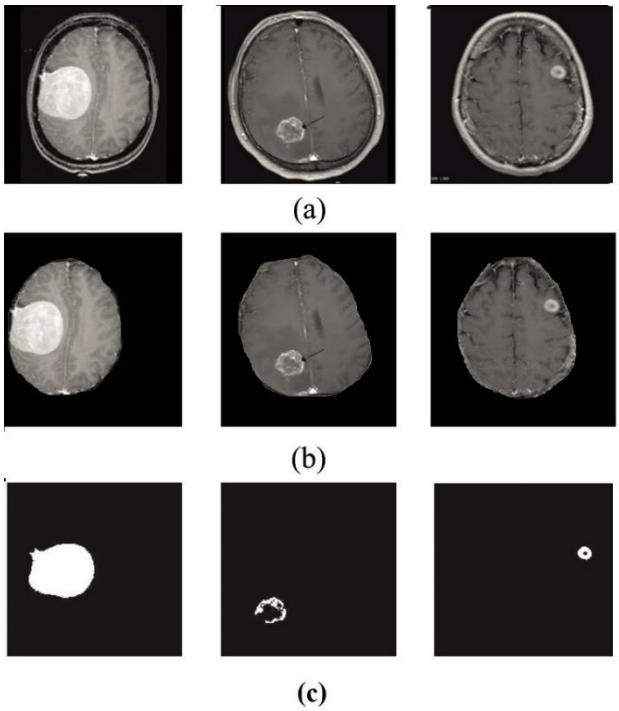

Fig. 2 a) Original Image b) Preprocessed Image c) Segmented Image

Fig. 2 visualizes the outcome produced by the OKE-ANFIS model on the applied MRI images. Fig. 2a illustrates the original MRI images and Fig. 2b denotes the preprocessed versions of the applied MRI images. Finally, Fig. 2c illustrates the segmented portions of the MRI images denoting the affected tumor regions in the target image.

Table 1 offers a comprehensive segmentation results analysis of the OKE based segmented technique under various MRI images. Fig. 3 investigates the MSE and RMSE analysis of the OKE based segmentation model under varying images. The figure portrayed that the OKE model has gained effective outcome by offering the least MSE and RMSE values. For instance, on the applied test image 1, the OKE model has achieved a minimum MSE of 0.154 and RMSE of 0.392. Besides, on the applied test image 3, the OKE method has achieved a lesser MSE of 0.109 and RMSE of 0.330. Also, on the applied test image 5, the OKE model has reached a lower MSE of 0.087 and RMSE of 0.295. Additionally, on the applied test image 7, the OKE technique has obtained a minimal MSE of 0.111 and RMSE of 0.333. Moreover, on the applied test image 9, the OKE approach has reached a lower MSE of 0.103 and RMSE of 0.324.

Table 1: Result Analysis of Proposed OKE Based Segmentation Method in terms of Different Measures

No. of Images	**MSE**	**RMSE**	**PSNR**	**JI**	**Accuracy**
Image 1	0.154	0.392	56.256	0.866	96.195
Image 2	0.109	0.330	57.757	0.834	97.358

Image 3	0.155	0.394	56.227	0.828	96.115
Image 4	0.101	0.318	58.088	0.851	97.399
Image 5	0.087	0.295	58.731	0.880	98.000
Image 6	0.126	0.355	57.127	0.866	97.481
Image 7	0.111	0.333	57.678	0.875	97.531
Image 8	0.129	0.359	57.025	0.851	96.781
Image 9	0.103	0.321	58.002	0.871	97.529
Image 10	0.105	0.324	57.919	0.864	97.464
Average	**0.118**	**0.342**	**57.481**	**0.859**	**97.185**

Fig. 4 examines the PSNR analysis of the presented OKE model for different MRI images. The figure demonstrated that the OKE model has resulted in a maximum PSNR value on the applied images. For instance, on the applied image 1, the OKE model has achieved a higher PSNR of 56.256dB. Likewise, on the applied image 3, the OKE technique has obtained a superior PSNR of 56.227dB. Similarly, on the applied image 5, the OKE manner has reached a maximum PSNR of 58.731dB. Simultaneously, on the applied image 7, the OKE model has achieved a higher PSNR of 57.025dB. Concurrently, on the applied image 9, the OKE methodology has obtained a superior PSNR of 58.002dB.

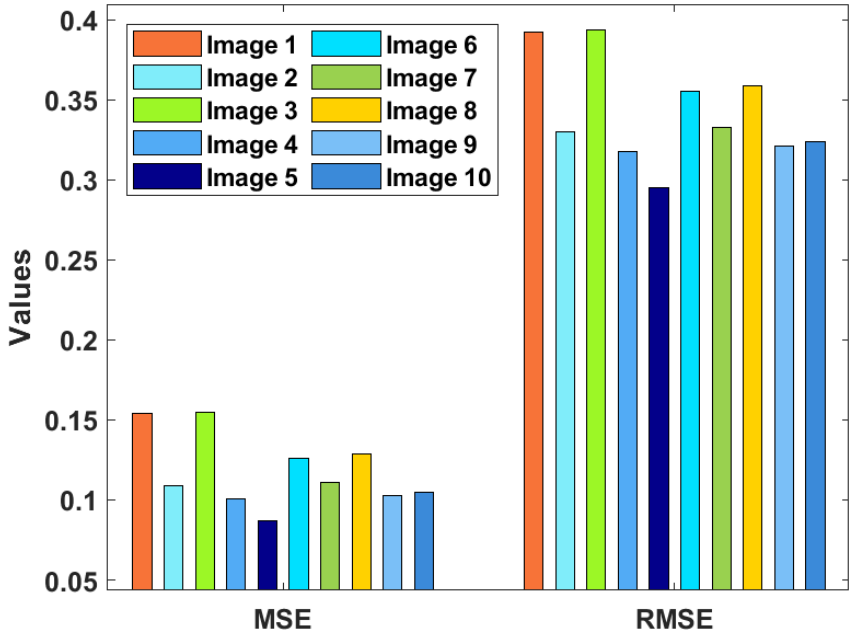

Fig. 3 MSE and RMSE analysis of OKE method with different MRI images

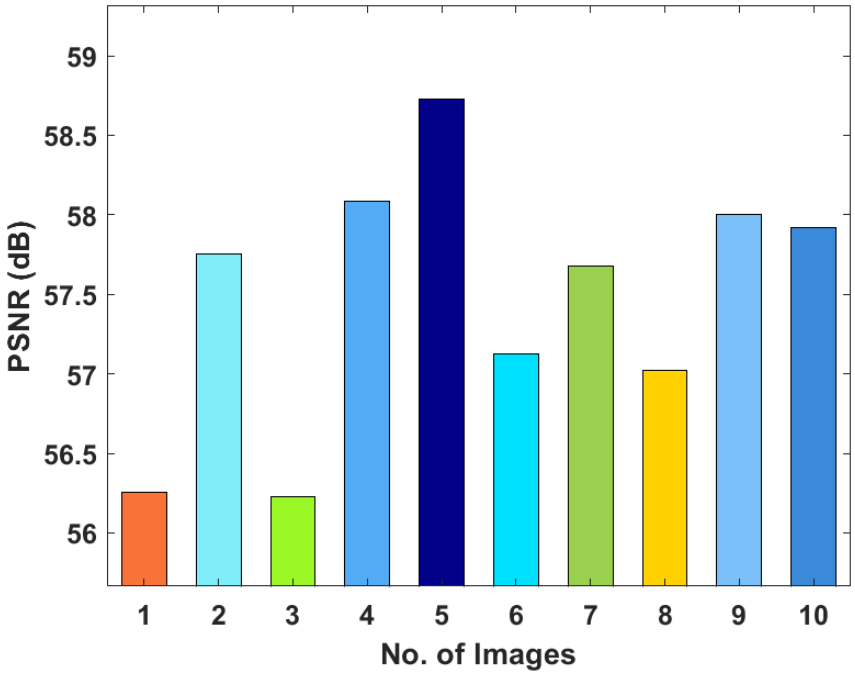

Fig. 4 PSNR analysis of OKE method with different MRI image

Fig. 5 determines the JI analysis of the proposed OKE method for distinct MRI images. The figure has shown that the OKE method has resulted in a superior JI value on the applied images. For instance, on the applied image 1, the OKE model has attained a maximum JI of 0.866. In addition, on the applied image 3, the OKE method has achieved a superior JI of 0.828. Along with that, on the applied image 5, the OKE algorithm has achieved a higher JI of 0.880. In line with, on the applied image 7, the OKE model has obtained a maximum JI of 0.875. Eventually, on the applied image 9, the OKE technique has reached a higher JI of 0.871.

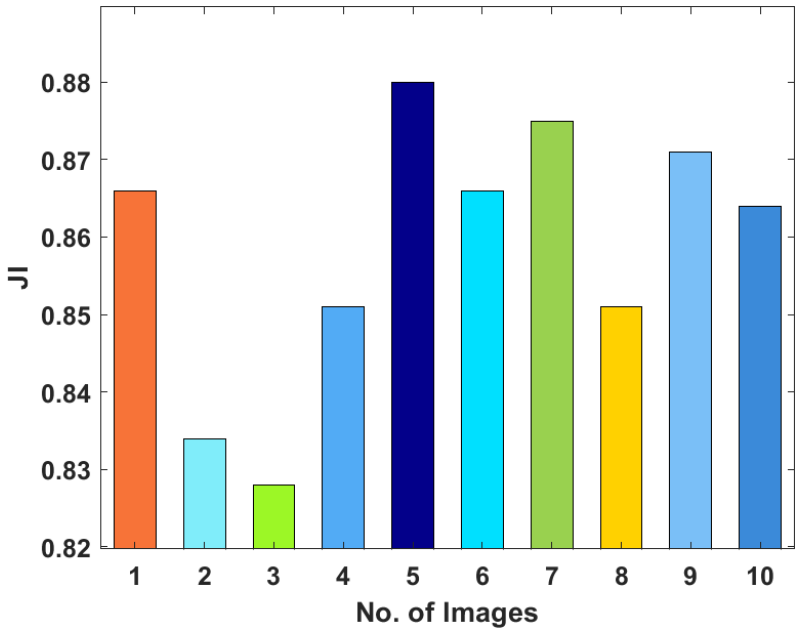

Fig. 5. JI analysis of OKE method with different MRI images

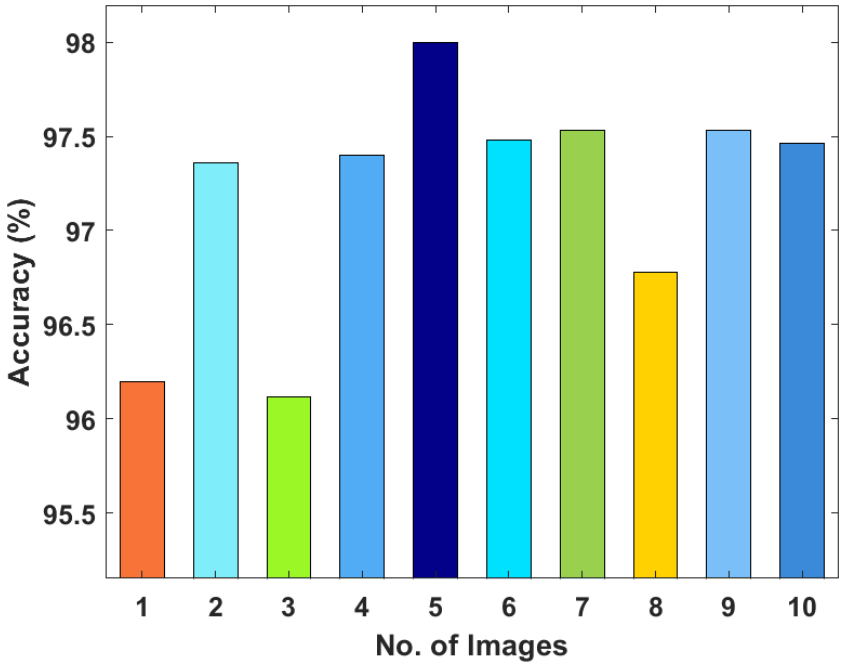

Fig. 6. Accuracy analysis of OKE method with different MRI images

Fig. 6 investigative the accuracy analysis of the projected OKE technique for several MRI images. The figure exhibited that the OKE method has resulted in a maximal accuracy value on the applied images. For instance, on the applied image 1, the OKE technique has achieved a maximum accuracy of 96.195%. In the same way, on the applied image 3, the OKE approach has attained a higher accuracy of 96.115%. Meanwhile, on the applied image 5, the OKE technique has reached a superior accuracy of 98%. Furthermore, on the applied image 7, the OKE model has achieved a higher accuracy of 97.531%. Moreover, on the applied image 9, the OKE methodology has achieved a higher accuracy of 97.529%.

Table 2 offers a comprehensive segmentation outcomes analysis of the OKE model with recent techniques interms of PSNR and JI [15]. Fig. 7 examines the PSNR analysis of the presented OKE model with other methods. The figure demonstrated that the TLBO-Tsallis model has exhibited that the ineffective result with least PSNR of 15.321dB. Likewise, the TLBO-Kapurs model has showcases the slightly increased result with PSNR of 15.718dB. At the same time, the TLBO-Shannon model has outperformed the moderate result with PSNR of 26.340dB. Finally, the proposed OKE model has portrayed that the maximum result with PSNR of 57.481dB.

Table 2: Segmentation Results of Proposed OKE-ANFIS with state of art methods in terms of PSNR and JI

Methods	**PSNR (dB)**	**JI**
Proposed OKE	57.481	0.859
TLBO-Kapurs	15.718	0.771
TLBO-Tsallis	15.321	0.742
TLBO-Shannon	26.340	0.837

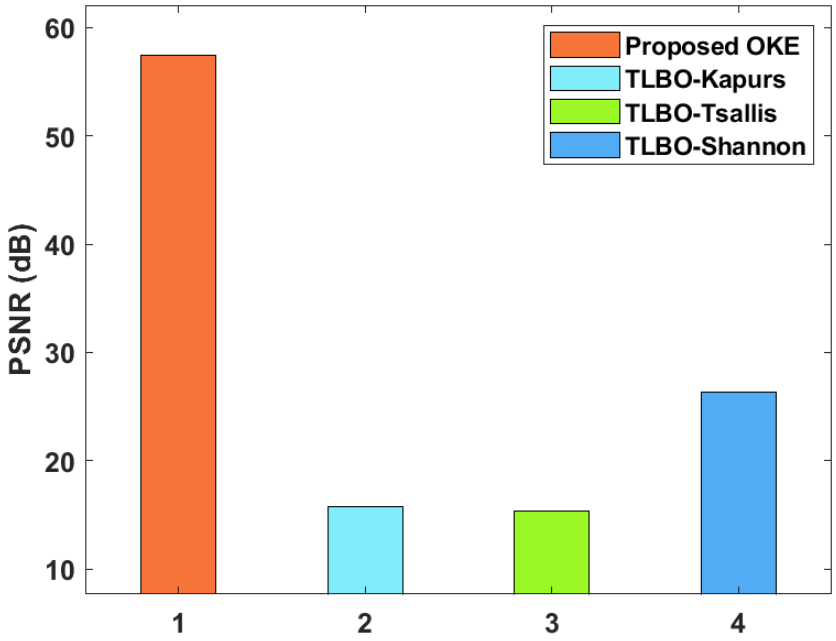

Fig. 7 Result analysis of OKE model interms of PSNR

Fig. 8 showcases the JI analysis of the proposed OKE method with other techniques. The figure has shown that the TLBO-Tsallis technique has outperformed that the ineffective outcome with the least JI of 0.742. Followed by, the TLBO-Kapurs approach has depicted somewhat higher outcomes with JI of 0.771. Concurrently, the TLBO-Shannon manner has exhibited a moderate result with JI of 0.837. At last, the proposed OKE algorithm has portrayed that the superior outcome with JI of 0.859.

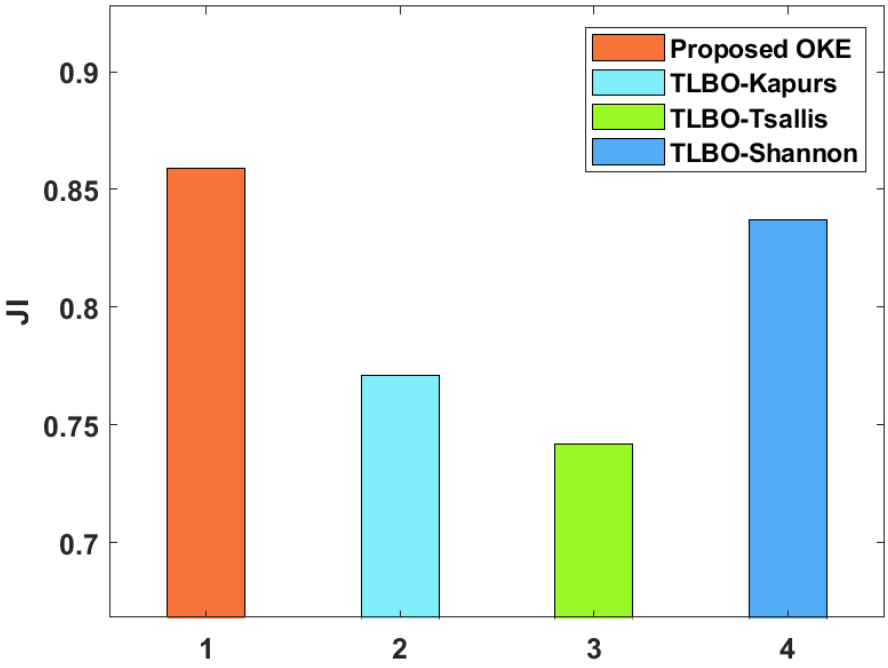

Fig. 8 Result analysis of OKE model interms of JI

Table 3 and Fig. 9 provides a comparative classification results analysis of the OKE-ANFIS model interms of distinct measures [16, 17]. From the experimental outcome, it is apparent that

the CNN model has failed to exhibit better classification with the sensitivity, specificity, and accuracy of 91.2%, 93.4%, and 93.3% respectively. Followed by, the MM-DCNN model has obtained slightly enhanced performance by offering a sensitivity, specificity, and accuracy of 92.6%, 93%, and 93.3%. Besides, the AS-CNN model has tried to show moderate outcomes by obtaining a sensitivity, specificity, and accuracy of 94.2%, 94.4%, and 94.6% respectively. Along with that, the Modified AdaBoost model has showcased somewhat acceptable outcomes with sensitivity, specificity, and accuracy of 94.3%, 95.1%, and 95.9% respectively.

Table 3: Comparisons of Proposed OKE-ANFIS with state of art methods on Classification Results

Methods	**Sensitivity**	**Specificity**	**Accuracy**
OKE-ANFIS	97.89	98.91	98.52
D-CNN	97.17	98.77	98.07
ANFIS	96.20	95.10	96.40
CNN	91.20	93.40	93.30
AS-CNN	94.20	94.40	94.60
MM-DCNN	92.60	93.00	93.30
Modified AdaBoost	94.30	95.10	95.90

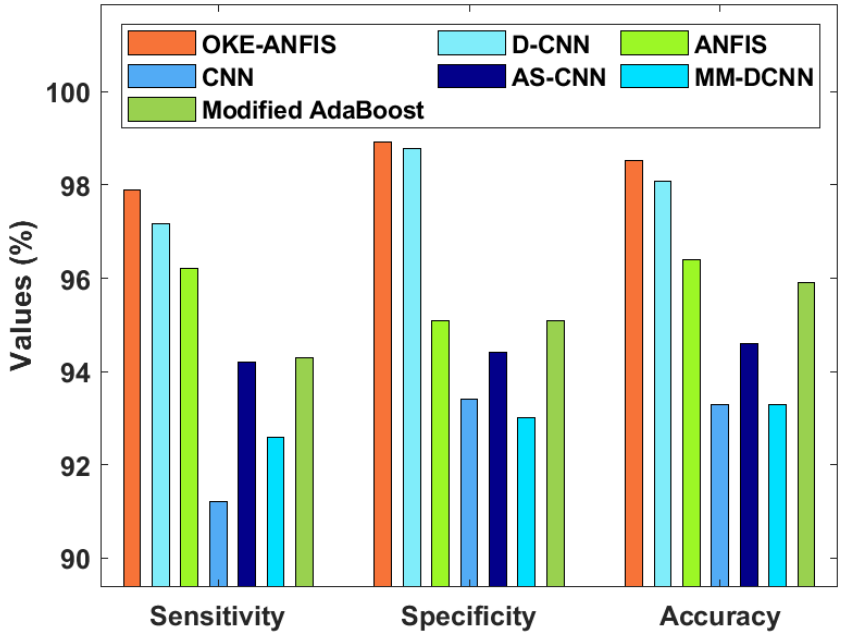

Fig. 9 Comparative analysis of OKE-ANFIS model with different measures

Simultaneously, the ANFIS model has resulted in a reasonable performance with the sensitivity, specificity, and accuracy of 96.2%, 95.1%, and 96.4%. At the same time, a competitive classification performance with the sensitivity, specificity, and accuracy of 97.17%, 98.77%, and 98.07% has been offered by the D-CNN model. However, the OKE-

ANFIS model has demonstrated effectual classification outcome with the maximum sensitivity, specificity, and accuracy of 97.89%, 98.91%, and 98.52%.

4. CONCLUSIONS

This paper has designed a novel OKE-ANFIS model for BT segmentation and classification using MRI images. The presented model involves skull stripping based preprocessing, segmentation, and classification. Primarily, the OKE-ANFIS model initially performs the skull stripping process as the preprocessing stage. Next, the preprocessed image undergoes OKE with MFO algorithm-based image segmentation process to identify the affected portions in the MRI image. Finally, the HOG based feature extraction and ANFIS classifier get executed to allocate the proper class labels of the applied MRI test image. To ensure the goodness of the OKE-ANFIS model, a wide range of simulations were performed and the results are investigated under several aspects. As a part of future scope, the performance of the OKE-ANFIS model can be improvised using the advanced DL architectures.

5. REFERENCES

[1] R. L. Siegel, K. D. Miller, and A. Jemal, "Cancer statistics, 2016," CA: A Cancer Journal for Clinicians, vol. 66, no. 1, pp. 7–30, 2016.
[2] J. Liu, M. Li, J.Wang, F.Wu, T. Liu, and Y. Pan, "A survey of MRIbased brain tumor segmentation methods," Tsinghua Science and Technology, vol. 19, no. 6, pp. 578–595, 2014.
[3] S. Bauer, R. Wiest, L. P. Nolte, and M. Reyes, "A survey of MRI based medical image analysis for brain tumor studies," Physics in Medicine & Biology, vol. 58, no. 13, pp. 97–129, 2013.
[4] G. Helms, K. Kallenberg, and P. Dechent, "Contrast-driven approach to intracranial segmentation using a combination of T2- and T1-weighted 3D MRI data sets," Journal of Magnetic Resonance Imaging, vol. 24, no. 4, pp. 790–795, 2006.
[5] P. Gibbs, D. Buckley, S. Blackb, and A. Horsman, "Tumour determination from MR images by morphological segmentation," Physics in Medicine & Biology, vol. 41, no. 11, pp. 2437– 2446, 1996.
[6] A. Stadlbauer, E. Moser, S. Gruber et al., "Improved delineation of brain tumors: An automated method for segmentation based on pathologic changes of 1H-MRSI metabolites in gliomas," NeuroImage, vol. 23, no. 2, pp. 454–461, 2004.
[7] M. Kass, A.Witkin, and D. Terzopoulos, "Snakes: active contour models," International Journal of Computer Vision, vol. 1, no. 4, pp. 321–331, 1988.
[8] A.A. Abdullah, B.S. Chize, Z. Zakaria, Design of cellular neural network (CNN) simulator based on matlab for brain tumor detection, J. Med. Imaging Health Inform. 2 (3) (2012) 296–306
[9] B.Goossens Despotovic, W. Philips, MRI segmentation of the human brain: challenges, methods, and applications, Comput. Math. Methods Med. 23 (2015).
[10] M. Havaei, A. Davy, D. Warde-Farley, A. Biard, A. Courville, Y. Bengio, C. Pal, P.M. Jodoin, H. Larochelle, Brain tumor segmentation with deep neural networks, Med. Image Anal. 35 (2017) 18–31.
[11] S. Pereira, A. Pinto, V. Alves, C.A. Silva, Brain tumor segmentation using convolutional neural networks in MRI images, IEEE Trans. Med. Imaging. (2016).

[12] S. Mirjalili, Moth-flame optimization algorithm: a novel nature-inspired heuristic paradigm, Knowl.-Based Syst. 89 (2015) 228–249.
[13] Jain, P. and Saxena, A., 2019. An opposition theory enabled moth flame optimizer for strategic bidding in uniform spot energy market. Engineering Science and Technology, an International Journal, 22(4), pp.1047-1067.
[14] https://www.cancerimagingarchive.net/
[15] Rajinikanth, V., Satapathy, S.C., Fernandes, S.L. and Nachiappan, S., 2017. Entropy based segmentation of tumor from brain MR images–a study with teaching learning based optimization. Pattern Recognition Letters, 94, pp.87-95.
[16] Selvapandian, A. and Manivannan, K., 2018. Fusion based glioma brain tumor detection and segmentation using ANFIS classification. Computer methods and programs in biomedicine, 166, pp.33-38.
[17] Ganesan, M., Sivakumar, N. and Thirumaran, M., 2020. Internet of medical things with cloud-based e-health services for brain tumour detection model using deep convolution neural network. Electronic Government, an International Journal, 16(1-2), pp.69-83.
[18] Shankar, K., Elhoseny, M., Lakshmanaprabu, S. K., Ilayaraja, M., Vidhyavathi, R. M., Elsoud, M. A., & Alkhambashi, M. (2020). Optimal feature level fusion based ANFIS classifier for brain MRI image classification. CONCURRENCY AND COMPUTATION-PRACTICE & EXPERIENCE, 32(1).
[19] Anupama, C. S. S., Sivaram, M., Lydia, E. L., Gupta, D., & Shankar, K. (2020). Synergic deep learning model–based automated detection and classification of brain intracranial hemorrhage images in wearable networks. Personal and Ubiquitous Computing, 1-10.
[20] Mohamed Elhoseny, K. Shankar, "Optimal Bilateral Filter and Convolutional Neural Network based Denoising Method of Medical Image Measurements", Measurement, Volume 143, Pages 125-135, September 2019.
[21] Lakshmanaprabu S.K, Sachi Nandan Mohanty, Sheeba Rani S, Sujatha Krishnamoorthy, Uthayakumar J, K. Shankar, "Online clinical decision support system using optimal deep neural networks", Applied Soft Computing, Volume 81, Page(s): 1-10, August 2019.
[22] Lakshmanaprabu S.K, Sachi Nandan Mohanty, K. Shankar, Arunkumar N, Gustavo Ramireze, "Optimal deep learning model for classification of lung cancer on CT images", Future Generation Computer Systems, Volume 92, Pages 374-382, March 2019.
[23] Joshua Samuel Raj, S. Jeya Shobana, Irina Valeryevna Pustokhina, Denis Alexandrovich Pustokhin, Deepak Gupta, K. Shankar, "Optimal Feature Selection based Medical Image Classification using Deep Learning Model in Internet of Medical Things", IEEE Access, Volume: 8, Issue:1, Page(s): 58006-58017, December 2020.
[24] Sikkandar, M. Y., Alrasheadi, B. A., Prakash, N. B., Hemalakshmi, G. R., Mohanarathinam, A., & Shankar, K. (2020). Deep learning based an automated skin lesion segmentation and intelligent classification model. Journal of Ambient Intelligence and Humanized Computing, 1-11.